Towards Real-Time Classification of Finger Movement Direction Using Encephalography Independent Components

Mohamed Mounir Tellache, Hiroyuki Kambara, Yasuharu Koike, Makoto Miyakoshi, Natsue Yoshimura

***Abstract*—**This study explores the practicality of using electroencephalographic (EEG) independent components to predict eight-direction finger movements in pseudo-real-time. Six healthy participants with individual-head MRI images performed finger movements in eight directions with two different arm configurations. The analysis was performed in two stages. The first stage consisted of using independent component analysis (ICA) to separate the signals representing brain activity from non-brain activity signals and to obtain the unmixing matrix. The resulting independent components (ICs) were checked, and those reflecting brain-activity were selected. Finally, the time series of the selected ICs were used to predict eight finger-movement directions using Sparse Logistic Regression (SLR). The second stage consisted of using the previously obtained unmixing matrix, the selected ICs, and the model obtained by applying SLR to classify a different EEG dataset. This method was applied to two different settings, namely the single-participant level and the group-level. For the single-participant level, the EEG dataset used in the first stage and the EEG dataset used in the second stage originated from the same participant. For the group-level, the EEG datasets used in the first stage were constructed by temporally concatenating each combination without repetition of the EEG datasets of five participants out of six, whereas the EEG dataset used in the second stage originated from the remaining participants. The average test classification results across datasets (mean ± S.D.) were 38.62 ± 8.36% for the single-participant, which was significantly higher than the chance level (12.50 ± 0.01%), and 27.26 ± 4.39% for the group-level which was also significantly higher than the chance level (12.49% ± 0.01%). The classification accuracy within [–45°, 45°] of the true direction is 70.03 ± 8.14% for single-participant and 62.63 ± 6.07% for group-level which may be promising for some real-life applications. Clustering and contribution analyses further revealed the brain regions involved in finger movement and the temporal aspect of their contribution to the classification. These results showed the possibility of using the ICA-based method in combination with other methods to build a real-time system to control prostheses.

Mohamed Mounir Tellache is with School of Engineering, Tokyo Institute of Technology, 4259 Nagatsutacho, Midori Ward, Yokohama, Kanagawa 226-8503 (phone: +818095722115; fax: +81-45-924-5066; e-mail: tellache.m.aa@m.titech.ac.jp).

Hiroyuki Kambara and Yasuharu Koike are with Institute of Innovative Research, Tokyo Institute of Technology, 4259 Nagatsutacho, Midori Ward, Yokohama, Kanagawa 226-8503 (e-mail: hkambara@hi.pi.titech.ac.jp, koike@pi.titech.ac.jp).

Makoto Miyakoshi is with Swartz Center for Computational Neuroscience, Institute for Neural Computation, University of California San Diego, CA, US (e-mail: mmiyakoshi@ucsd.edu).

Natsue Yoshimura is with Institute of Innovative Research, Tokyo Institute of Technology, 4259 Nagatsutacho, Midori Ward, Yokohama, Kanagawa 226-8503. She is also with PRESTO, JST, Japan (e-mail: yoshimura.n.ac@m.titech.ac.jp).

***Keywords*—**Brain-computer interface, BCI, electroencephalography, EEG, finger motion decoding, independent component analysis, pseudo-real-time motion decoding.

I. Introduction

LOSING a limb can drastically alter one's life due to the inability to perform day to day tasks. Paralysis due to injuries in the spinal cord can also limit one's ability and in worse cases lose one's autonomy. Development in prostheses presents hope in regaining some sort of normal life. Brain-computer interfaces (BCI) are investigated as methods to control prostheses [1]. Invasive methods involve implanting electrodes in the brain or signal amplifiers at the nerve endings to acquire clear signals to achieve the desired control precision [2]. However, due to the complexity of surgical procedures and long-term instability, non-invasive methods are gaining more traction. Electromyography (EMG) is relatively easier to record and translate into control commands but can be limited to the number of available muscles to record from. It is also difficult to obtain reliable signals in cases of motor impairment, spinal cord injury, and locked-in syndrome. An alternative is EEG which can record brain activity at high temporal resolution from the surface of the head. Furthermore, EEG sensors are portable and commercially available. Many studies have used EEG for motion control [3]-[7].

Since EEG electrodes are placed on the scalp, each electrode records the activity of a mixture of brain sources, which leads to a low spatial resolution. EEG signals also have low amplitude and are often contaminated with noise from eye movements, muscle artifacts, and so on. Another issue with EEG-based BCI is reusability and transferability from one person to the other. Placement of electrodes is likely to vary from one session to the next within the same participant. When dealing with multiple subject analysis, differences in the brain anatomy affect the conductance and therefore affect the recorded EEG. Solving these issues will lead to building a reliable BCI.

ICA is widely used to unmix brain-activity signals from artifacts [8]-[10]. The scalp topographies of the ICs obtained from ICA can be represented by equivalent dipoles which will localize the ICs in the brain [11] and thus mitigate the issue of low spatial resolution. For the reusability issue, it has been shown that ICA decomposition is stable across sessions recorded at different periods within-subject [12]. Other studies validated the possibility of temporally concatenating EEG recordings of different participants for group-ICA [13], [14]. This suggests that a combination of ICA and an appropriate

machine learning algorithm can result in a modular system that can predict motion directions on newly recorded EEG data within-individual and across different individuals. However, to the extent of the authors' knowledge, this approach has not been fully investigated yet.

This study aims to investigate the possibility of using the ICA-based decoding method for real-time application. Using an eight-direction center-out finger movement task, movement directions were estimated from EEG data by applying the unmixing matrix obtained from ICA and a machine learning model obtained from a different dataset originating from either the same participant or a different participant. The brain regions involved in finger-movement were also localized and a classification contribution analysis was performed.

II. Materials and Methods

A. Participants

Six healthy participants performed the experiment (two females and four males). With a mean age of M = 40.67 years and SD = 7.23. The study protocol was approved by the ethics committee of the University of California, San Diego (Approval No. 14353) and carried out in accordance with the Declaration of Helsinki. Written informed consent was obtained from each participant before the experiment.

B. Experiment

The experiment was designed to separate the effect of the extrinsic and intrinsic coordinate frames. The extrinsic coordinate frame represents the position of an object in space while the intrinsic coordinate frame is a body-centered frame that is related to and moves with a specific body part such as a joint or muscle [15]. It has been shown that the extrinsic coordinate frame is transformed into the intrinsic coordinate frame in certain regions in the brain during motor control [16]. The experimental design referred to in this study was first applied in an invasive study on monkeys [15] and further validated in a human study [17].

Participants sat on a chair with their forearm and wrist supported and a PC screen was in front of them. They moved their index finger on a touchpad from the center of a circle to one of eight directions indicated on the screen. The eight targets are positioned on the circumference where the angle between every two consecutive targets is 45 degrees. Each participant performed a total of 1,280 trials divided into 40 sessions. The participants changed their elbow angle after every 10 sessions alternating between 0º and 90º. This elbow angle alternation dissociated the intrinsic and extrinsic coordinate frame in the classification analysis described later. Each trial consisted of two seconds of rest, then the target appears for two seconds. The participants were instructed to perform a single motion to the target regardless of whether the cursor reaches the target. Cursor position was recorded at a sampling rate of 30Hz.

C. Data Acquisition

EEG was recorded from 128 channels using Biosemi active two amplifier system (Biosemi, Amsterdam, Netherlands). Muscle activity onset was detected using EMG sensors placed over the right extensor indicis and flexor digitorum. EEG and EMG signals were recorded at a sampling rate of 2,048 Hz. The 3D positions of the EEG sensors, the nasion, left pre-auricular point and, right pre-auricular were measured using a posture functional capacity evaluation system. (zebris Medical GmbH, Isny, Germany).

D. MRI Image Acquisition and Preprocessing

MRI images were used to generate an accurate forward electric model to better localize the equivalent dipoles for each participant. The MRI images were acquired using a General Electric (GE) Discovery MR750 3.0 T equipped with a 32-channel receiver coil. A sagittal image was acquired using a T1-weighted spoiled gradient recalled sequence (TR = 8.132 s; TE = 3.192 ms; FA = 8°; FOV = 256 ×256 mm; matrix size = 256 × 256; 172 slices; slice thickness = 1.2 mm). The MRI images were used for DIPFIT as a custom MRI image. Images were normalized to the standard MNI brain template using SPM12 (https://www.fil.ion.ucl.ac.uk/spm/).

E. EEG Preprocessing

Raw EEG data were loaded into EEGLAB toolbox 2019.1, MATLAB R2017b for further processing. Data were filtered to eliminate baseline drift, line noise at 60 Hz, and frequencies of non-interest. Frequencies between 1 Hz and 40 Hz were kept. Data were then down-sampled to 512 Hz and channel signals were checked in a semi-automatic way and noisy channels - any channels that exceed [–500 μv 500 μv] for more than 20% of the time were removed. Channels were then re-referenced to the average. For better ICs decomposition, data were epoched to one second before the target appears and 2 seconds after as shown in Fig. 1 (a). For single-participant ICA (Fig. 1 (b)), datasets were divided into two sets with an equal number of trials in each set, and ICA was applied to each dataset separately using adaptive mixture ICA (AMICA) [18]. For group-level ICA (Fig. 1 (c)), datasets of all participants were down-sampled to 256 Hz and each unique combination of the datasets of five participants out of six was temporally concatenated. ICA was then applied to the concatenated sets.

F. ICs Localization and Selection

To localize the ICs in the brain we used EEGLAB plugin DIPFIT v3.3. The single-participant ICA used participant-specific channel locations as well as individual head MRI images for an accurate electric forward model. For group-level ICA, the standard MRI image provided with the toolbox was used. The ICs selection process was done in a semi-automated manner.

EEGLAB plugin ICLabel [19] predicts if the IC represents brain activity, eye or muscle artifacts, and so on. ICs were then manually checked in search of properties inherent to brain activity. In particular, event-related potential (ERP), relevant peaks in the power spectrum, the position of the equivalent dipole, and the residual variance that remains after the fitting. The threshold for residual variance was initially set to 30%. ICs with more than a 70% chance of representing brain activity

were kept regardless of the residual variance.

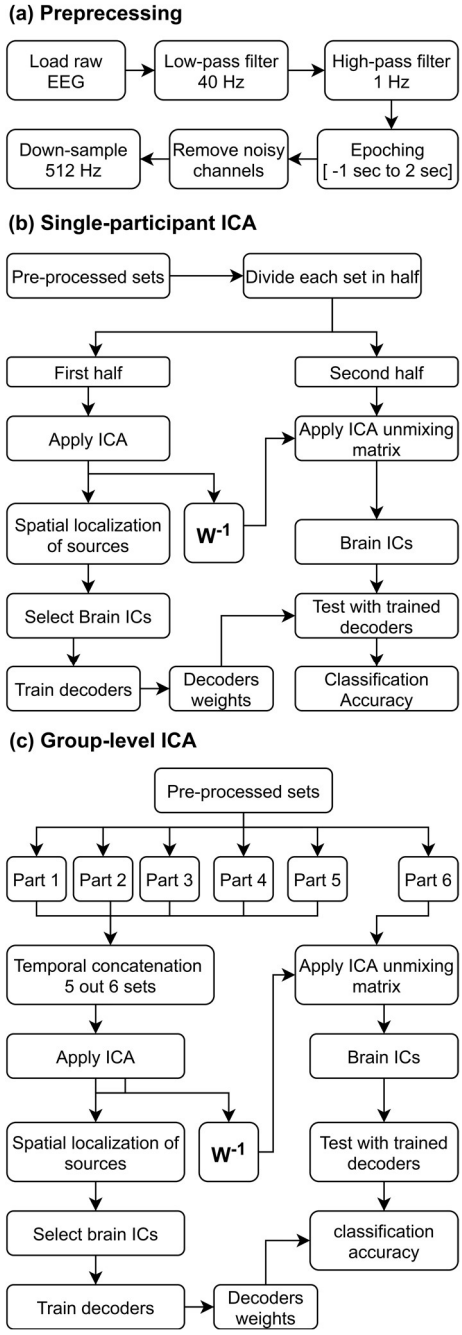

Fig. 1 Flowchart of the study. (a) preprocessing steps of raw EEG signals. (b) Single-participant ICA. (c) Group-level ICA

G.Eight-Directions Finger Movement Classification and Testing

SLR with Laplace approximation (SLR toolbox ver 1.51 https://bicr.atr.jp//~oyamashi/SLR_WEB.html) was used to predict eight-finger movement directions [20]. This algorithm was used in many studies [17], [20], [21] for both fMRI and EEG data decoding mainly for its ability to automatically select the important features. The classifiers were trained using the concatenated time series of the ICs where zero to one second after the stimulus of each ICs was used. Due to the computational cost of SLR, the input was down-sampled to 64 Hz. To predict finger movement direction in the extrinsic coordinate frame, the trials where the finger moved to the same target were labeled with the same label regardless of the elbow angle resulting in trials where the finger performed different actions (extension vs adduction) being labeled the same. The training was performed using leave-one-out cross-validation. For each single-participant set, leave-one-out cross-validation consisted of 80 folds and for each of the temporally concatenated sets, leave-one-out cross-validation consisted of 800 folds. The performance of the classifiers was evaluated on the test sets. The trials were divided into bins where each bin contains a single trial of each direction without repeat. Each bin was then used once as a validation set and 79 times (799 times) in the training set for the single-participant sets (for the concatenated sets).

The test sets were constructed as follows: ICA relates EEG times series and ICs time series by a mixing matrix W such that $\mathrm{EEG} = \mathrm{W} \times \mathrm{IC}$. The unmixing matrix is then the inverse of W such that $\mathrm{IC} = \mathrm{W}^{-1} \times \mathrm{EEG}$ .For single-participant ICA, for every participant let Set_n be the EEG set for 'participant n' and Set_{1n} and Set_{2n} be the two halves of Set_n, $\mathrm{test}_{1n}$and test_{2n}be the test sets. $\mathrm{IC}_{1n} = {\mathrm{W}_{1n}}^{-1} \times \mathrm{Set}_{1n}$ and $\mathrm{IC}_{2n} = {\mathrm{W}_{2n}}^{-1} \times \mathrm{Set}_{2n}$. The test sets are then: $\mathrm{test}_{1n} = {\mathrm{W}_{1n}}^{-1} \times \mathrm{Set}_{2n}$ *and* $\mathrm{test}_{2n} = {\mathrm{W}_{2n}}^{-1} \times \mathrm{Set}_{1n}$.

For group-level ICA, let $\mathrm{GroupSet}_n$ be the EEG set constructed from temporally concatenating all participants' EEG except 'participant n'. $\mathrm{GroupSet}_n = \mathrm{GroupW}_n \times \mathrm{GroupIC}_n$ where $\mathrm{GroupW}_n$is the resulting mixing matrix. The test set is then $\mathrm{test}_n = {\mathrm{GroupW}_n}^{-1} \times \mathrm{Set}_n$

A non-parametric permutation test [22] was performed to evaluate the statistical significance of the classification results. Classifiers were trained with the same data using randomly generated labels to obtain accuracy distribution from the dataset, and *p*-values of the real-label dataset were calculated by evaluating the position of the real-label dataset in the distribution (Table I). Due to the computational cost, the permutation test was repeated 5000 times for the single-participant sets and 2500 times for the group-level temporally concatenated sets.

H.Clustering of ICs

The shape and size of the skull vary between individuals. Brains of different individuals also differ physiologically. This means that the same electrode may not record the same active brain regions across several individuals. To solve this issue, ICs were clustered based on the spatial properties of the equivalent dipoles using the EEGLAB study framework. The standard k-means algorithm was used [23]. Clustering was performed on the ICs obtained from the 12 single-participant sets, and on the ICs obtained from the 6 temporally concatenated group-level sets. The number of clusters is an open parameter and should be computed empirically. Each cluster should have at least 50% of unique sets in accordance with previous work [24]. This limited the maximum number of clusters to 15 for the temporally concatenated group-level sets and 23 for the single-participant

sets. The number of clusters was then varied to evaluate the stability of the results. The results were stable from 10 to 15 for the temporally concatenated sets and 12 to 18 for the single-participant sets. To balance the spatial resolution and the number of unique sets in each cluster, the number of clusters was 13 for the temporally concatenated sets and 16 for the single-participant sets. Each cluster contained 91.03% (SD = 0.97%) of the concatenated sets and 70.83% (SD = 2.13%) of the single-participant sets. The centroid of each cluster was located in the AAL atlas [25].

TABLE I
SINGLE-PARTICIPANT ICA RESULTS

Part1						
Participants	1	2	3	4	5	6
Second Set classification Acc%	47.21	38.62	39.94	46.14	37.78	27.66
Random Label Second Set %	12.51	12.48	12.48	12.49	12.51	12.49
Adjacent Error %	30.90	31.75	30.70	29.97	29.46	33.06
Accuracy Within [–45° 45°] %	78.10	70.37	70.64	76.11	67.24	60.71
P-value Second Set	p < 2.00e-04	p < 2.00e-04	p < 2.00e-04	p < 2.00e-04	p < 2.00e-04	p < 2.00e-04
Part2						
Participants	1	2	3	4	5	6
First Set Classification Acc%	55.16	35.33	29.97	45.78	33.45	26.42
Random Label First Set %	12.5	12.52	12.5	12.5	12.51	12.51
Adjacent Error %	27.95	36.54	27.64	33.60	30.71	34.61
Accuracy Within [–45° 45°] %	83.11	71.87	57.61	79.38	64.16	61.03
P-value First Set	p < 2.00e-04	p < 2.00e-04	p < 2.00e-04	p < 2.00e-04	p < 2.00e-04	p < 2.00e-04

TABLE II
GROUP-LEVEL ICA RESULTS

Set	12345	12346	12356	12456	13456	23456
6th participant's Acc %	28.58	32.24	26.30	19.08	25.74	31.62
Random Labels 6th participant's Acc %	12.48	12.49	12.50	12.49	12.51	12.49
Adjacent Error %	39.15	35.34	34.45	32.75	34.32	36.21
Accuracy Within [–45° 45°] %	70.77	61.08	53.53	59.06	66.56	64.80
P-value Unseen Data	p < 4.00e-04	p < 4.00e-04	p < 4.00e-04	p < 4.00e-04	p < 4.00e-04	p < 4.00e-04

I. Classification Weight-Matrices Analysis

SLR automatically selects the important features for the classification. By analyzing the weight matrices of the classifiers, the clusters most contributive to the classification can be defined and the time periods that were used for the classification can be localized. Each cluster $Clst(t)$ is composed of "n" ICs where $Clst(t) = \frac{1}{n}\sum_{i=1}^{n} IC_i(t)$ where $IC_n(t)$ is the time series of IC_n. Let $Imp_n(t_0)$ be the importance of a time point $IC_n(t_0)$ to the classification. The importance of a time point is defined by the number of classifiers that selected the time point averaged over the cross-validations ($Imp_n(t_0) = \frac{1}{m}\sum_{i=1}^{m} k$) where "m" is the number of cross-validation runs, "k" is the number of classifiers that chose $IC_n(t_0)$ for the classification in a single cross-validation run.

Let $cluster_k(t_0)$ be the importance of $cluster_k$ at time t_0 where $cluster_k(t_0) = \frac{1}{n}\sum_{i=1}^{n} Imp_i(t_0)$. The importance of $cluster_k$ is then the mean importance of its data points. The contribution of each cluster is the ratio of its importance over the total importance of all the clusters.

III. RESULTS

A. ICs Analysis

ICA decomposition for single-participant sets resulted in 128 ICs for each participant except for Participant 3 which had 127 ICs due to the removal of one noisy channel. Out of 1,790 ICs, only 261 were kept after rejecting ICs that represented non-brain signals and ICs where the noise was dominant. The number of accepted ICs ranged from 14 to 38 per dataset. For group-level ICA, the noisy channel of Participant 3 needed to be removed from all datasets due to temporal concatenation resulting in 127 ICs for each dataset. Out of 762 ICs, only 150 were kept. The number of ICs per dataset ranged from 20 to 28. The residual variance is a measure of how well the dipole fit models the data. It is the difference between the projected scalp map from the fitted dipole and the actual scalp map. All the selected ICs from the group-level ICA had a residual variance lower than 30%. For the single-participant ICA, some ICs exceeded the threshold of 30% but were included in the next step because they showed other properties that reflect brain activity such as peaks in the power spectrum at relevant frequencies between 5 Hz and 30 Hz and especially around 10 Hz, a clear ERP response and, ICLabel predicted with more than 70% certainty that they represent brain-activity.

B. Eight-Directions Finger Movement Classification

The classification accuracy of the test sets averaged over the cross-validation runs is shown in Table I for the single-participant ICA and Table II for the group-level ICA. The average classification accuracy of the permutation test is also shown along with the p-values of the null hypothesis that the observed classification accuracy is due to random chance. The

classification accuracy was significantly higher than the chance level ($p < 2.00e-04$ for single-participant ICA and $p < 4.00e-04$ for group-level ICA). Confusion matrix tables (supplementary Fig. 6 for single-participant sets part1, Fig. 7 for single-participant sets part2, and Fig. 8 for temporally concatenated sets) were analyzed to check if there was any pattern in the false-positives. The number of correctly classified trials and false-positives in each direction is shown in Fig. 2 for the single-participant ICA and Fig. 3 for the group-level ICA. The percentage of the adjacent false-positives and the classification accuracy within –45°, 45° of the intended direction is also shown in Table I.

C. Clustering and Contribution Results

The ICs of the 12 single-participant sets were clustered into 16 clusters and the ICs of the 6 temporally combined sets were clustered into 13 clusters. The contribution to the classification of each cluster was computed and the centroid of each cluster was located in the AAL atlas (Fig. 9 for single-participant ICA and Fig. 10 for group-level ICA). For the single-participant sets, the clusters were located in the left lingual, the right superior occipital gyrus, the left precuneus, the right middle temporal gyrus, the right cerebellum crus1, the left fusiform, the right precuneus, the right middle frontal gyrus orbital part, the right superior parietal gyrus, the left middle temporal gyrus, the left precentral gyrus, the left superior frontal gyrus dorsolateral, the right superior temporal gyrus, the left paracentral lobule, the right superior frontal gyrus dorsolateral, and the left median cingulate gyrus in descending order of contribution to the classification. For the group-level ICA, the clusters were in the left lingual, the left inferior occipital gyrus, the right inferior occipital gyrus, the right precuneus, the right postcentral gyrus, the left middle frontal gyrus, the left supramarginal gyrus, the right superior parietal gyrus, the left supplementary motor area (SMA), the left cuneus 1, the left cuneus 2, the right superior temporal gyrus, and the left superior parietal gyrus in descending order of contribution. The importance to the classification of each time point of the cluster is shown in Fig. 4 (a) for single-participant ICA and Fig. 5 (a) for group-level ICA. To further understand the temporal transition of the importance to the classification, the importance of each four consecutive time points was averaged. The time periods of interest are from the cue onset at t = 0 s to the EMG onset around t = 220 ms and from the EMG onset to the cursor onset around t = 450 ms. The results are shown in Fig. 4 (b) for the single-participant ICA and Fig. 5 (b) for the group-level ICA. Ten out of 16 clusters for the single-participant ICA and 11 out of 13 clusters for the group-level ICA were most contributive at t1 = [125 ms to 187.5 ms] before the EMG onset.

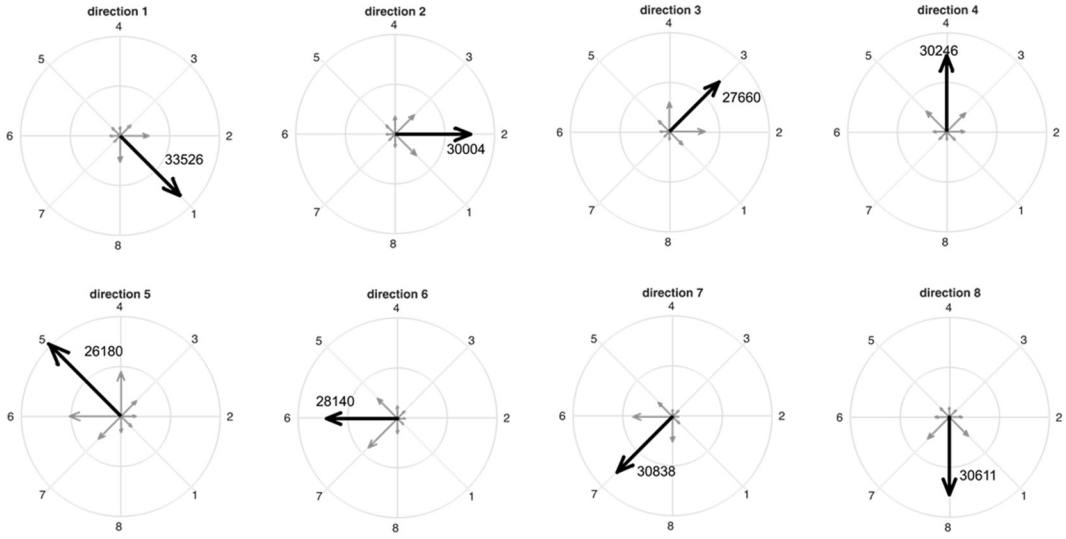

Fig. 2 The number of true-positives and false-positive for each direction for the single-participant ICA. The magnitude of the arrows reflects the number of trials. The dark arrow represents the true direction and the gray arrows represent the false-positives

IV. Discussion

This study aims to elucidate the possibility of using EEG-ICs to predict eight finger movement directions in a real-time prediction manner. In particular, the possibility of using the unmixing matrix W^{-1} that was obtained from applying ICA to an initial set to extract ICs from a different set and predict the finger movement direction of the latter set using classifiers trained using the ICs of the initial set. Single-participant ICA refers to when the set used for obtaining W^{-1} and training the classifiers and the set used for testing originated from the same participant while group-level ICA refers to when the set used for obtaining W^{-1} and training the classifier consisted of the temporal concatenation of five sets originating from five different participants while the test set originated from a different participant. Using ICA to unmix brain-signals from other signals of non-interest minimizes the effect of eye movement and other artifacts which allows the classifiers to utilize information related to motion from brain activity. Applying ICA and training a model every time to classify finger motion directions is computationally expensive which makes it not suitable for real-life applications. Therefore, there is value in exploring the possibility of predicting finger

movement direction from an EEG set using the ICA unmixing matrix and the machine learning model that has been trained on a different set. First, this method was applied to data originating from the same participant. The average test classification accuracy from 12 unique training datasets is 38.62 ± 8.36% which was significantly higher (p < 2.00e-04) than classification accuracy from models trained with random labels (12.50 ± 0.01%). In the second part of this study, ICA unmixing matrix and the classifiers were trained using temporally concatenated EEG sets originating from five participants and tested on the remaining sixth participant. The average test accuracy was 27.26 ± 4.39%. The results were lower than the single-participant results but still significantly higher (p < 4.00e-04) than the chance level (12.49 ± 0.01%). Further evaluation of the confusion tables showed that false-positives were concentrated on adjacent directions to the true direction which makes the accuracy of the classifiers within [–45°, 45°] of the true direction 70.03 ± 8.14% for single-participant ICA and 62.63 ± 6.07% for group-level ICA.

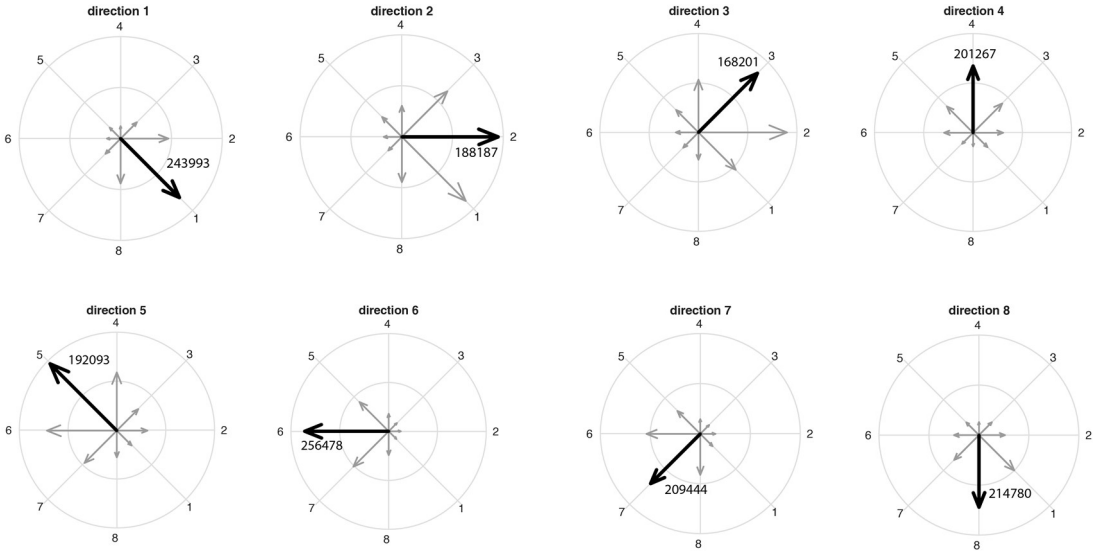

Fig. 3 The number of true-positives and false-positive for each direction for the group-level ICA. The magnitude of the arrows reflects the number of trials. The dark arrow represents the true direction and the gray arrows represent the false-positives

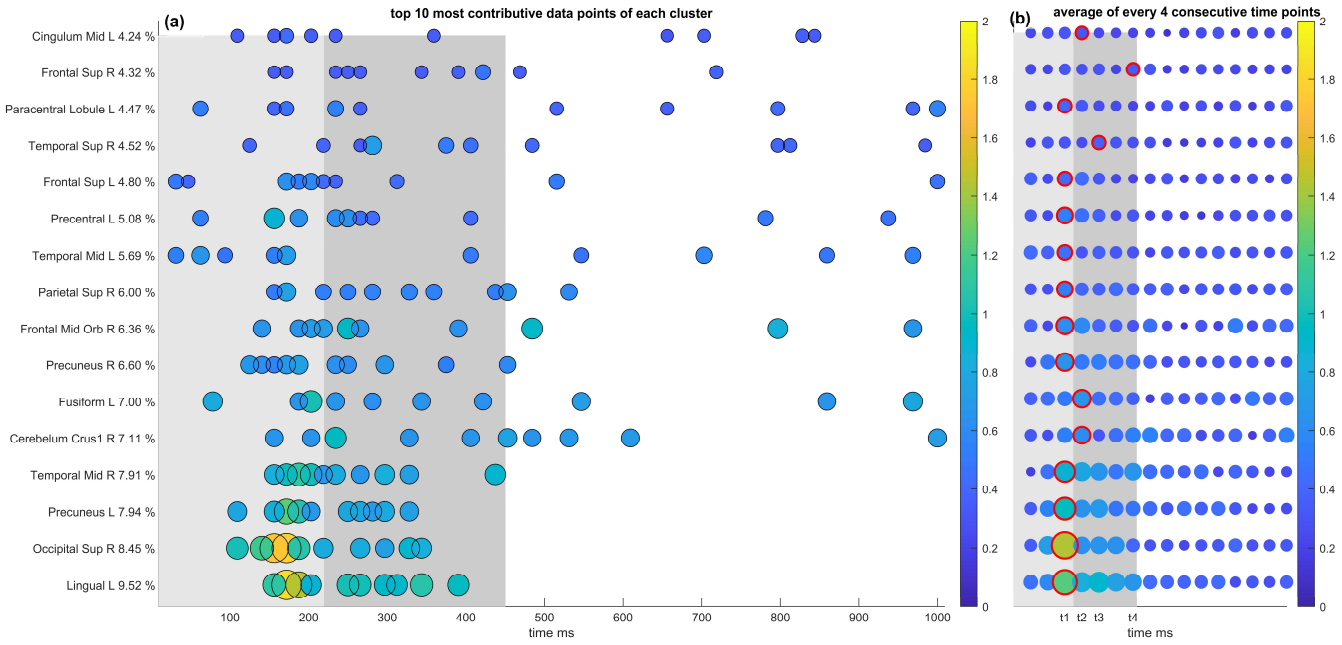

Fig. 4 The clusters of the single-participant ICA. (a) The importance of each data point of each cluster. (b) The average of each four consecutive data points of (a). The clusters are in descending order of contribution. The contribution of each cluster is indicated next to its name. The size and color of each point represent its importance. The unit of the color bar is the number of classifiers that selected the data point averaged over the number of ICs per cluster. The light-shaded area represents the time period between the cue onset at t = 0 ms and the EMG onset at t = 220 ms. The dark-shaded area represents the time period between the EMG onset at t = 220 ms and the cursor onset at t = 450 ms. t_1= [125 ms to 187.5 ms], t_2= [187.5 ms to 250 ms], t_3= [250 ms to 312.5 ms], t_4= [375 ms to 437.5 ms]

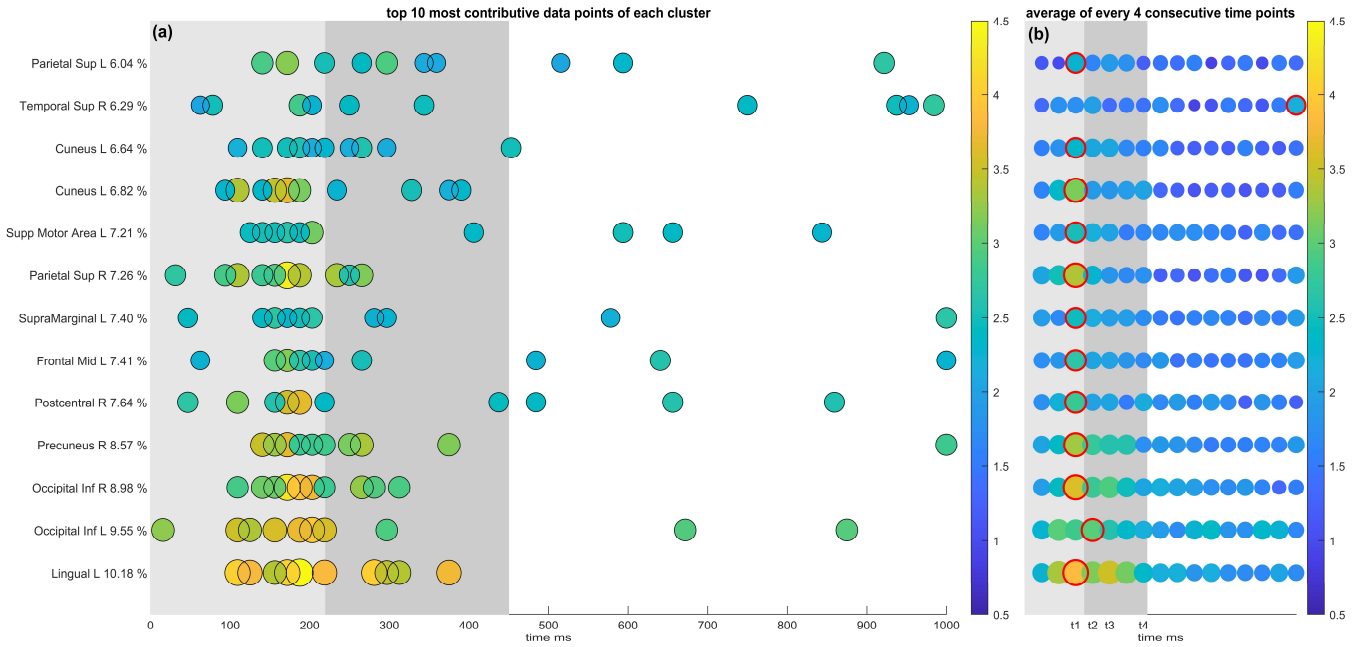

Fig. 5 The clusters of the group-level ICA. (a) The importance of each data point of each cluster. (b) The average of each four consecutive data points of (a). The clusters are in descending order of contribution. The contribution of each cluster is indicated next to its name. The size and color of each point represent its importance. The unit of the color bar is the number of classifiers that selected the data point averaged over the number of ICs per cluster. The light-shaded area represents the time period between the cue onset at t = 0s and the EMG onset at t = 220ms. The dark-shaded area represents the time period between the EMG onset at t = 220 ms and the cursor onset at t = 450 ms. t_1= [125 ms to 187.5 ms], t_2= [187.5 ms to 250 ms], t_3= [250 ms to 312.5 ms], t_4= [375 ms to 437.5 ms]

Most BCI studies focus on large body parts such as classifying simple hand movements [4] and binary reaching tasks [9]. The literature about finger movement classification is very limited and even more so for classifying 8 finger movements. Some studies focused on predicting which finger is moving like [26] where they decoded five finger motions with 54% accuracy while some other studies tried to decode single finger movements. Binary finger movement classification was achieved with 77.11% accuracy in [5] and left vs right index finger movement was classified with 62% accuracy in [27]. One study [28] dealt with classifying four thumb movements achieved an accuracy of 64.6± 3.6. All the previous studies were done offline and the performance in a real-time application was not assessed. For online studies, a cursor could be moved to the right or left with an average accuracy of 75% using invasive electrocorticogram (ECoG) signals [29]. Another study [30] achieved online discrimination between right vs left index finger movement to move a target in the screen to the left or the right with 80% accuracy in seven out of ten participants. Four motions (wrist flexion, extension, and all fingers open, close) were classified from the EEG signal with 78.44% classification accuracy [31]. This study realized the discrimination of eight classes of movement of the same finger where the classification accuracy at the single-participant level is comparable to the classification accuracy of fewer classes in the present literature. Furthermore, to the best of the authors' knowledge, the group-level ICA results are novel and have not been addressed before. The current accuracy may be suitable for some real-life BCI applications.

The clustering analysis revealed the brain regions that were involved in finger movement and the contribution analysis revealed the importance of each cluster and the temporal aspect of the contribution to the classification. 22 out of 29 clusters were most contributive at $t_1 = [125 \text{ ms to } 187.5 \text{ ms}]$ before the EMG onset. The most contributing clusters belonged to the left lingual, the right superior occipital gyrus, the left precuneus, and the right middle temporal gyrus for the single-participant ICA and the left lingual, left inferior occipital gyrus, the right inferior occipital gyrus, and the right precuneus for the group-level ICA. Some of these areas such as the lingual [32] are involved in visuospatial processing which is reasonable. The inferior occipital gyrus is a part of the dorsal visual pathway and the precuneus that is involved in motor coordination that requires shifting attention when making movements [33]. Areas that are involved in motor execution were also observed such as the precentral gyrus (M1) and SMA

This study is a first step towards building a real-time eight-finger movement classification system. Future work would be to evaluate the classification accuracy of real-time EEG.

V. Supplementary Figures

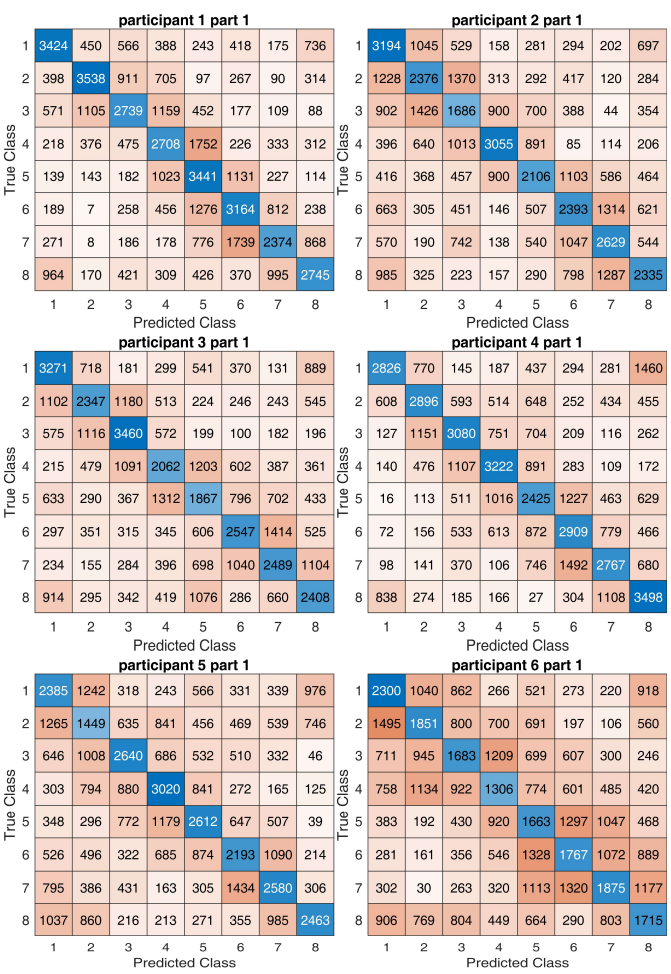

Fig. 6 Confusion tables of the single-participant ICA sets of all participants part 1

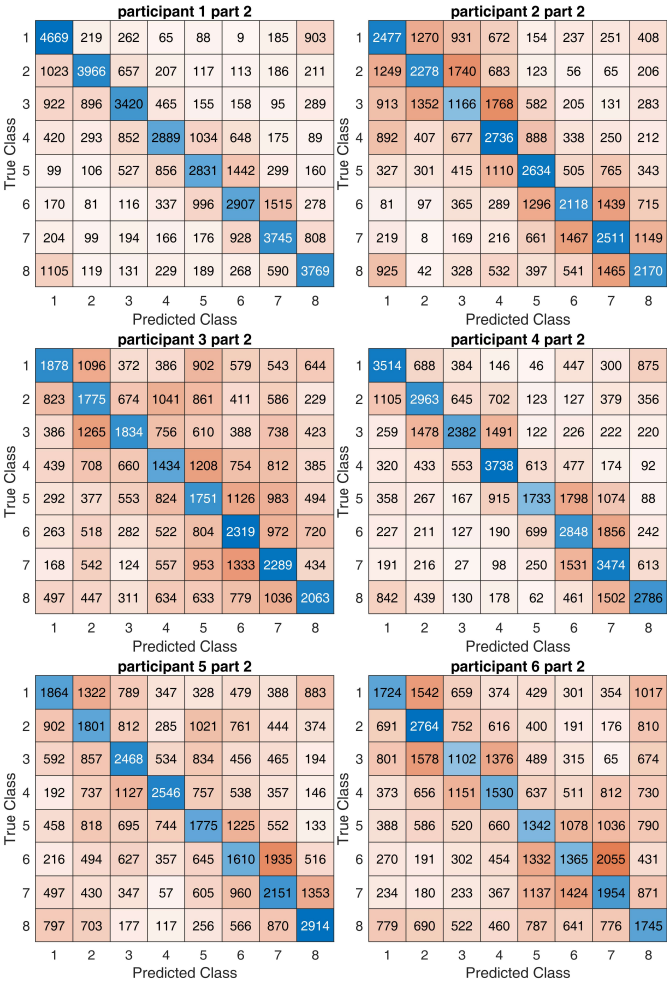

Fig. 7 Confusion tables of the single-participant ICA sets of all participants part 2

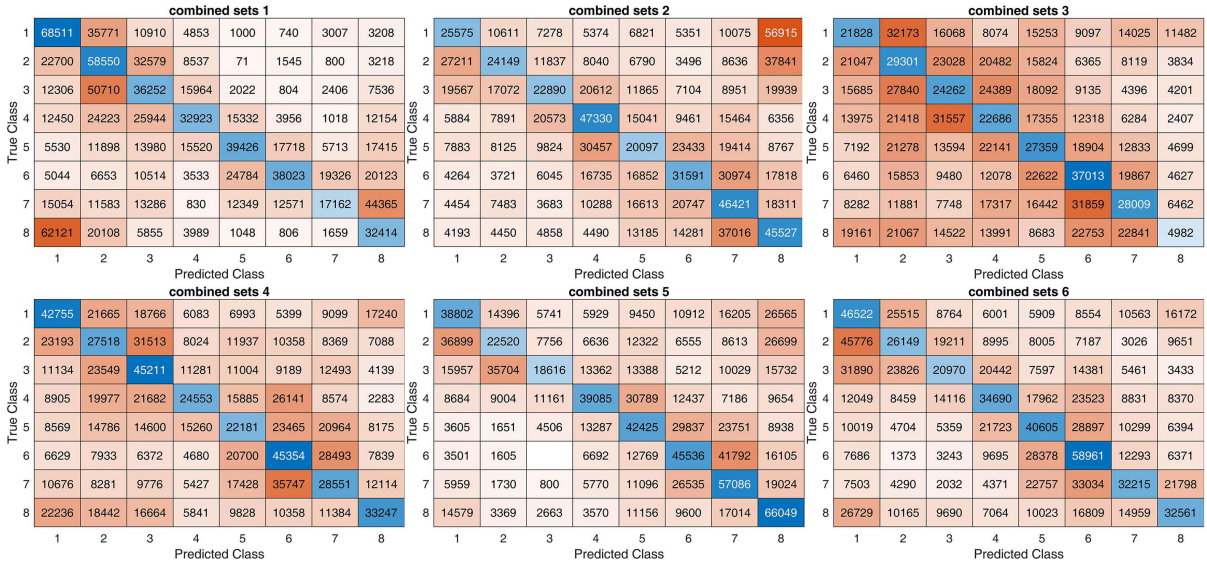

Fig. 8 Confusion tables of the group-level ICA sets

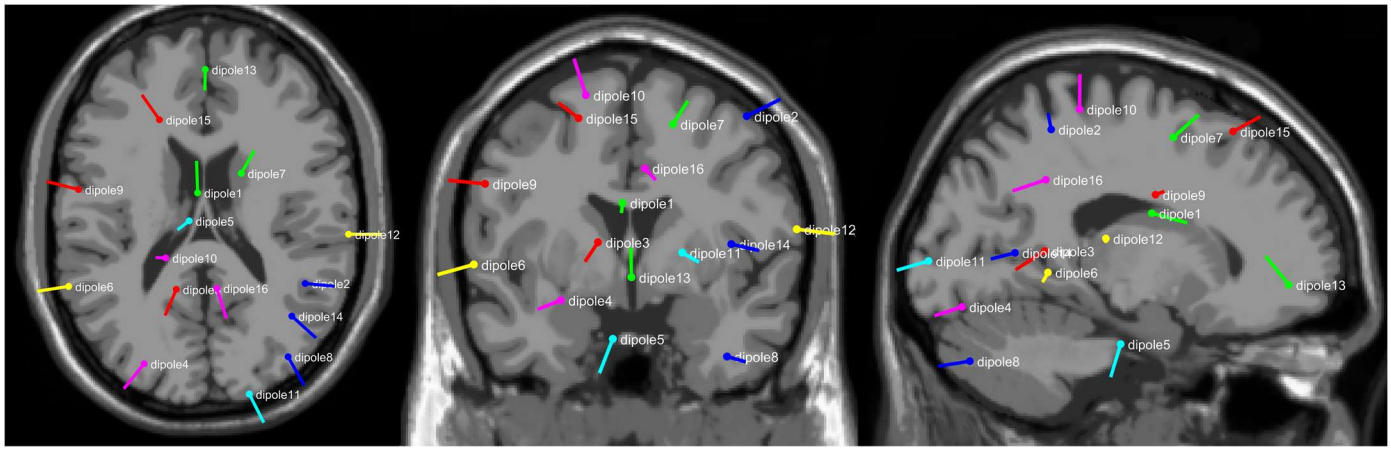

Fig. 9 Locations of the centroids of the single-participant ICA clusters

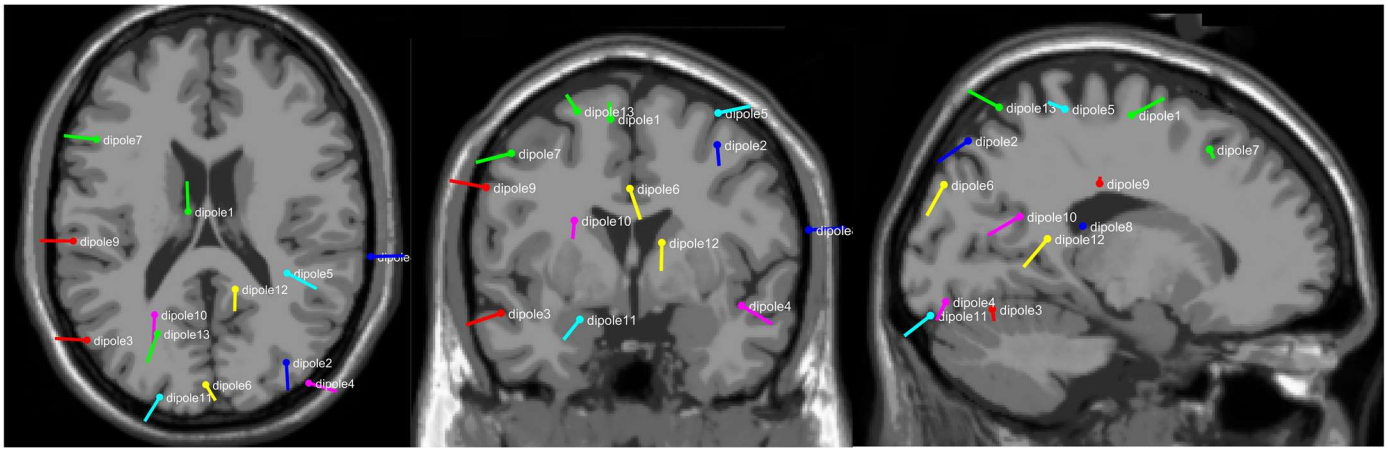

Fig. 10 Location of the centroids of the group-level ICA clusters

FUNDING

This work is supported by the Program for Advancing Strategic International Networks to Accelerate the Circulation of Talented Researchers from JSPS, The Swartz Foundation (Old Field, NY) through Swartz Center for Computational Neuroscience in The University of California San Diego. This work was also supported in part by JST PRESTO (Precursory Research for Embryonic Science and Technology) (grant number JPMJPR17JA)

REFERENCES

[1] J. J. Shih, D. J. Krusienski, and J. R. Wolpaw, "Brain-computer interfaces in medicine," *Mayo Clin. Proc.*, vol. 87, no. 3, pp. 268–279, 2012, doi: 10.1016/j.mayocp.2011.12.008.

[2] P. P. Vu *et al.*, "A regenerative peripheral nerve interface allows real-time control of an artificial hand in upper limb amputees," *Sci. Transl. Med.*, vol. 12, no. 533, pp. 1–12, 2020, doi: 10.1126/scitranslmed.aay2857.

[3] D. J. McFarland, W. A. Sarnacki, and J. R. Wolpaw, "Electroencephalographic (EEG) control of three-dimensional movement," *J. Neural Eng.*, vol. 7, no. 3, p. 36007, Jun. 2010, doi: 10.1088/1741-2560/7/3/036007.

[4] N. Robinson, C. Guan, A. P. Vinod, K. Keng Ang, and K. Peng Tee, "Multi-class EEG classification of voluntary hand movement directions," *J. Neural Eng.*, vol. 10, no. 5, 2013, doi: 10.1088/1741-2560/10/5/056018.

[5] K. Liao, R. Xiao, J. Gonzalez, and L. Ding, "Decoding individual finger movements from one hand using human EEG signals," *PLoS One*, vol. 9, no. 1, pp. 1–12, 2014, doi: 10.1371/journal.pone.0085192.

[6] E. Y. L. Lew, R. Chavarriaga, S. Silvoni, and J. del R. Millán, "Single trial prediction of self-paced reaching directions from EEG signals," *Front. Neurosci.*, vol. 8, no. AUG, pp. 1–13, 2014, doi: 10.3389/fnins.2014.00222.

[7] J. Cho, J. Jeong, K. Shim, D. Kim, and S. Lee, "Classification of Hand Motions within EEG Signals for Non-Invasive BCI-Based Robot Hand Control," in *2018 IEEE International Conference on Systems, Man, and Cybernetics (SMC)*, 2018, pp. 515–518, doi: 10.1109/SMC.2018.00097.

[8] T.-P. Jung, S. Makeig, A. J. Bell, and T. J. Sejnowski, "Independent Component Analysis of Electroencephalographic and Event-Related Potential Data," in *Central Auditory Processing and Neural Modeling*, P. W. F. Poon and J. F. Brugge, Eds. Boston, MA: Springer US, 1998, pp. 189–197.

[9] Y. Wang and S. Makeig, "Predicting intended movement direction using EEG from human posterior parietal cortex," *Lect. Notes Comput. Sci. (including Subser. Lect. Notes Artif. Intell. Lect. Notes Bioinformatics)*, vol. 5638 LNAI, pp. 437–446, 2009, doi: 10.1007/978-3-642-02812-0_52.

[10] K. L. Snyder, J. E. Kline, H. J. Huang, and D. P. Ferris, "Independent component analysis of gait-related movement artifact recorded using EEG electrodes during treadmill walking," *Front. Hum. Neurosci.*, vol. 9, no. DEC, pp. 1–13, 2015, doi: 10.3389/fnhum.2015.00639.

[11] A. Delorme, J. Palmer, J. Onton, R. Oostenveld, and S. Makeig, "Independent EEG sources are dipolar," *PLoS One*, vol. 7, no. 2, 2012, doi: 10.1371/journal.pone.0030135.

[12] R. Grandchamp *et al.*, "Stability of ICA decomposition across within-subject EEG datasets . To cite this version : HAL Id : hal-00797464 Stability of ICA decomposition across within-subject EEG datasets," 2013.

[13] F. Cong *et al.*, "Validating rationale of group-level component analysis based on estimating number of sources in EEG through model order selection," *J. Neurosci. Methods*, vol. 212, no. 1, pp. 165–172, 2013, doi:

10.1016/j.jneumeth.2012.09.029.
[14] R. J. Huster, S. M. Plis, and V. D. Calhoun, "Group-level component analyses of EEG: Validation and evaluation," *Front. Neurosci.*, vol. 9, no. JUL, pp. 1–14, 2015, doi: 10.3389/fnins.2015.00254.
[15] S. Kakei, D. S. Hoffman, and P. L. Strick, "Sensorimotor transformations in cortical motor areas," *Neurosci. Res.*, vol. 46, no. 1, pp. 1–10, 2003, doi: 10.1016/S0168-0102(03)00031-2.
[16] Y. Fujiwara, J. Lee, T. Ishikawa, S. Kakei, and J. Izawa, "Diverse coordinate frames on sensorimotor areas in visuomotor transformation," *Sci. Rep.*, vol. 7, no. 1, p. 14950, 2017, doi: 10.1038/s41598-017-14579-3.
[17] N. Yoshimura, H. Tsuda, T. Kawase, H. Kambara, and Y. Koike, "Decoding finger movement in humans using synergy of EEG cortical current signals," *Sci. Rep.*, vol. 7, no. 1, pp. 1–11, 2017, doi: 10.1038/s41598-017-09770-5.
[18] J. Palmer, K. Kreutz-Delgado, and S. Makeig, "AMICA: An Adaptive Mixture of Independent Component Analyzers with Shared Components," *San Diego, CA Tech. report, Swart. Cent. Comput. Neurosci.*, pp. 1–15, 2011, [Online]. Available: http://sccn.ucsd.edu/~jason/amica_a.pdf%5Cnpapers2://publication/uuid/E6296FC1-7F6B-400C-85D0-3A292A27F710.
[19] L. Pion-Tonachini, K. Kreutz-Delgado, and S. Makeig, "ICLabel: An automated electroencephalographic independent component classifier, dataset, and website," *Neuroimage*, vol. 198, no. April, pp. 181–197, 2019, doi: 10.1016/j.neuroimage.2019.05.026.
[20] O. Yamashita, M. Sato, T. Yoshioka, F. Tong, and Y. Kamitani, "Sparse estimation automatically selects voxels relevant for the decoding of fMRI activity patterns.," *Neuroimage*, vol. 42, no. 4, pp. 1414–1429, Oct. 2008, doi: 10.1016/j.neuroimage.2008.05.050.
[21] N. Yoshimura *et al.*, "Dissociable neural representations of wrist motor coordinate frames in human motor cortices," *Neuroimage*, vol. 97, pp. 53–61, 2014, doi: 10.1016/j.neuroimage.2014.04.046.
[22] T. Nichols and A. Holmes, "Nonparametric Permutation Tests for Functional Neuroimaging," *Hum. Brain Funct. Second Ed.*, vol. 25, no. August 1999, pp. 887–910, 2003, doi: 10.1016/B978-012264841-0/50048-2.
[23] J. Onton and S. Makeig, "Information-based modeling of event-related brain dynamics.," *Prog. Brain Res.*, vol. 159, pp. 99–120, 2006, doi: 10.1016/S0079-6123(06)59007-7.
[24] H. Tanaka, M. Miyakoshi, and S. Makeig, "Dynamics of directional tuning and reference frames in humans: A high-density EEG study," *Sci. Rep.*, vol. 8, no. 1, pp. 1–18, 2018, doi: 10.1038/s41598-018-26609-9.
[25] E. T. Rolls, C.-C. Huang, C.-P. Lin, J. Feng, and M. Joliot, "Automated anatomical labelling atlas 3.," *Neuroimage*, vol. 206, p. 116189, Feb. 2020, doi: 10.1016/j.neuroimage.2019.116189.
[26] K. Anam, M. Nuh, and A. Al-Jumaily, "Comparison of EEG pattern recognition of motor imagery for finger movement classification," *Int. Conf. Electr. Eng. Comput. Sci. Informatics*, pp. 24–27, 2019, doi: 10.23919/EECSI48112.2019.8977037.
[27] T. Jia *et al.*, "Small-Dimension Feature Matrix Construction Method for Decoding Repetitive Finger Movements from Electroencephalogram Signals," *IEEE Access*, vol. 8, pp. 56060–56071, 2020, doi: 10.1109/ACCESS.2020.2982210.
[28] R. Alazrai, H. Alwanni, and M. I. Daoud, "EEG-based BCI system for decoding finger movements within the same hand," *Neurosci. Lett.*, vol. 698, pp. 113–120, 2019, doi: 10.1016/j.neulet.2018.12.045.
[29] T. Milekovic *et al.*, "An online brain-machine interface using decoding of movement direction from the human electrocorticogram," *J. Neural Eng.*, vol. 9, no. 4, 2012, doi: 10.1088/1741-2560/9/4/046003.
[30] J. Lehtonen, P. Jylänki, L. Kauhanen, and M. Sams, "Online classification of single EEG trials during finger movements," *IEEE Trans. Biomed. Eng.*, vol. 55, no. 2, pp. 713–720, 2008, doi: 10.1109/TBME.2007.912653.
[31] S. Bhattacharyya, M. Pal, A. Konar, and D. N. Tibarewala, "An interval type-2 fuzzy approach for real-time EEG-based control of wrist and finger movement," *Biomed. Signal Process. Control*, vol. 21, pp. 90–98, 2015, doi: 10.1016/j.bspc.2015.05.004.
[32] K. Whittingstall, M. Bernier, J. C. Houde, D. Fortin, and M. Descoteaux, "Structural network underlying visuospatial imagery in humans," *Cortex*, vol. 56, pp. 85–98, 2014, doi: 10.1016/j.cortex.2013.02.004.
[33] N. Wenderoth, F. Debaere, S. Sunaert, and S. P. Swinnen, "The role of anterior cingulate cortex and precuneus in the coordination of motor behaviour," *Eur. J. Neurosci.*, vol. 22, no. 1, pp. 235–246, 2005, doi: 10.1111/j.1460-9568.2005.04176.x.